# A Permeability-Based Model for Prediction of Freckling in Nickel Superalloy Single-Crystal Castings

NICK GREEN, ROGER REED, and DMYTRO SHEVCHENKO

Nickel superalloy single-crystal castings with dimensions representative of aero engine high-pressure turbine blades were manufactured to two casting conditions. Under conditions of low thermal gradient freckle chains of randomly oriented secondary grains arose on external casting surfaces. The number of freckle chains depended on the orientation of the crystal relative to the external casting surface. A permeability-based model of inward flow conductance through the semi-solid to sustain an upward rising plume of solute-enriched liquid at the mould wall forming a freckle is developed. The model accounts for both extrinsic casting and intrinsic material factors. It is discovered that by inclusion of the anisotropic permeability arising from the differing crystal orientations within individual castings and application of a new criterion for flow in the semi-solid, conductance to flow within the semi-solid local to the plume explains almost all variation in the number of freckles formed between individual castings. The model is applied to assess the effect of extrinsic and intrinsic parameters on flow conductance, ranking their relative significance.

https://doi.org/10.1007/s11661-026-08115-0


## I. INTRODUCTION

BUOYANT thermosolutal plumes of uprising partitioned interdendritic liquid are widely acknowledged as a source of freckle chains that are readily detectable, occurring commonly on external cast faces.[1] Plumes have been imaged directly in low-temperature binary alloys[2] and more recently, nickel superalloys.[3] In both cases, an inward flow of the overlying bulk liquid to the semi-solid region is required to sustain plumes. Local solidification conditions, thermal gradient, $G$, and liquidus isotherm velocity, $v$, expressed as cooling rate, are reported as having first-order effect on freckling, low $G.v$ of the order of 0.1 to 0.14 $Ks^{-1}$ defining an approximate threshold for this phenomenon.[4–6] Freckle formation is considered only possible when the fluid flow velocity within the mushy zone exceeds the rate of solid advance.[7] It is reported that the likelihood of freckling rises with increasing downward inclination of the liquidus isotherm relative to the external casting wall.[8]

The driving and retarding forces for freckling have commonly been rationalised using a Rayleigh-based criterion *e.g.*[9] This can be decomposed into driving force for solute flow arising from the acceleration due to gravity and density difference between partitioned interdendritic and bulk liquid $g\ (\Delta\rho/\rho_0)$ and mushy zone length to the source of the freckle ($h$) and permeability ($\kappa$) and the retarding forces of kinematic viscosity ($\eta$) and a damping force of thermal diffusivity ($\alpha$) Eq. [1].

$$Ra = \frac{g(\Delta\rho/\rho_0)h\kappa}{\eta\alpha} \qquad [1]$$

A ranking of composition-driven density difference between partitioned and bulk liquid has provided key insight in to the relative freckle defect susceptibility of alloys[10] and the role of microstructure on permeability, linking it to primary dendrite arm spacing,[11] with Karman–Kozeny model applied to account calculate permeability[12] with further refinement through inclusion of anisotropic permeability.[9] The role of crystal orientation on freckling in test bars[13] has previously led to conclusion that the ⟨001⟩ primary orientation aligned to the casting axis has the lowest resistance to vertical melt flow.

Microstructural models of solidification coupled with thermosolutally driven flow have been developed that consider local more global phenomena.[14] These highlight the sensitivity of the flow to crystal orientation and

NICK GREEN, ROGER REED, and DMYTRO SHEVCHENKO are with the High Temperature Research Centre, University of Birmingham, Birmingham B15 2TT, UK. Contact e-mail: nick.green@htrc.bham.ac.uk
Manuscript submitted September 30, 2025; accepted January 6, 2026.



Published online: 05 March 2026

diffuse flow pathways. Similarly, phase field modelling of microstructure has been applied[15] to realise improved models of anisotropic permeability.

The motivation of the research reported in this paper is to establish the significance of the anisotropic permeability of the semi-solid, through which the inward flow of fluid sustaining plumes is resisted, on the extent of freckling under otherwise nominally constant casting and solidification conditions in a pseudo-turbine blade. The arising experimental data are applied to inform development of an improved model of permeability for possible application in freckle criterion functions, and subsequently applied to deconvolve the significance of microstructural and casting parameters on the likelihood of freckling.

## II. EXPERIMENTAL METHODS

CMSX-4 nickel superalloy single-crystal castings of a geometric analogue to a high-pressure turbine blade were investment cast in a Bridgman furnace using casting parameters typical of those applied in aerospace production facilities. Sixteen parts were arranged circumferentially as a wax assembly, Figures 1(a) and (b), and shelled to create a zircon-silica-alumina mould typical of single-crystal casting of nominal thickness 6 mm. Multiple moulds were produced and cast to either of two conditions in a Bridgman single-crystal casting furnace. Baffle clearance was adapted to be either sufficiently close to suppress freckling (3 mm nominal clearance to external profile with enclosing fingers, referred to subsequently as a tight baffle), or far enough to create freckle chains on the external faces of the sections representative of the root block (round, open baffle) Figure 1(c). Single crystals were obtained using a helical grain eliminator connecting individual starter blocks with the bases of each casting so as to yield a wide range of growth orientations within the components. Key casting parameters are set out in Table I. After casting samples were blasted clean and electrochemically etched to reveal any freckle chains formed. Castings containing bicrystals were discarded.

The numbers and locations of freckles arising on each face were recorded after grain etching and visual inspection and the orientation of the primary growth direction of the main grain relative to the external face measured using the Laue X-ray back reflection method. Both inclination, $\gamma$, and twist, $\delta$, to the external face were determined with an estimated measurement precision of 1 deg. Figure 2 shows the sense of the $\langle 001 \rangle$ growth direction measurement relative to the external cast face of interest.

## III. EXPERIMENTAL RESULTS

Here, we report the experimental results obtained and explore their relationships to elucidate the key factors affecting freckling response under nominally identical solidification conditions.

Two distinctly different outcomes were realised in the experiments.

There was a complete absence of freckle chains in castings produced using the tight baffle. However, on the external root section face of all castings produced

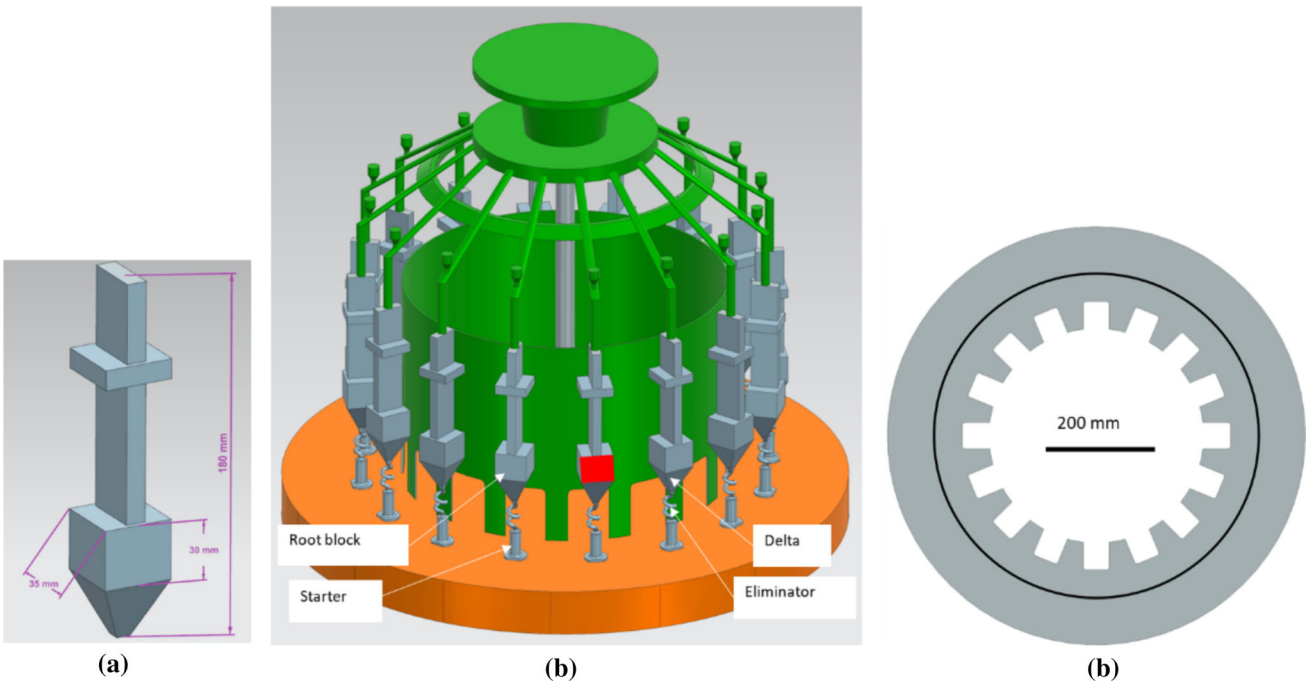


Fig. 1—(*a*) Wax assembly model showing high pressure turbine blade analogues arranged circumferentially with top filling system, starter blocks, helical grain eliminators, delta, and root block. Freckle chains arise on the root block faces of width 35 mm and height 30 mm, example highlighted in red, (*b*) component geometry, and (*c*) tight (grey) and open (black circle) baffle profiles.

Table I. Casting Parameters and Casting Process Setup

| | |
|---|---|
| Alloy composition (Nominal CMSX-4) (Weight Pct) | Ni (balance), Cr 6.5, Co 9.6, W 6.4, Ta 6.5, Re 3.0, Al 5.6, Ti 1.0, Hf 0.1, Mo 0.6 |
| Hot zone temperature | 1520 °C |
| Withdrawal velocity | 63 $\mu$ms$^{-1}$ |
| Shell material | zircon + silica |
| Shell thickness (Nominal) | 6 mm |

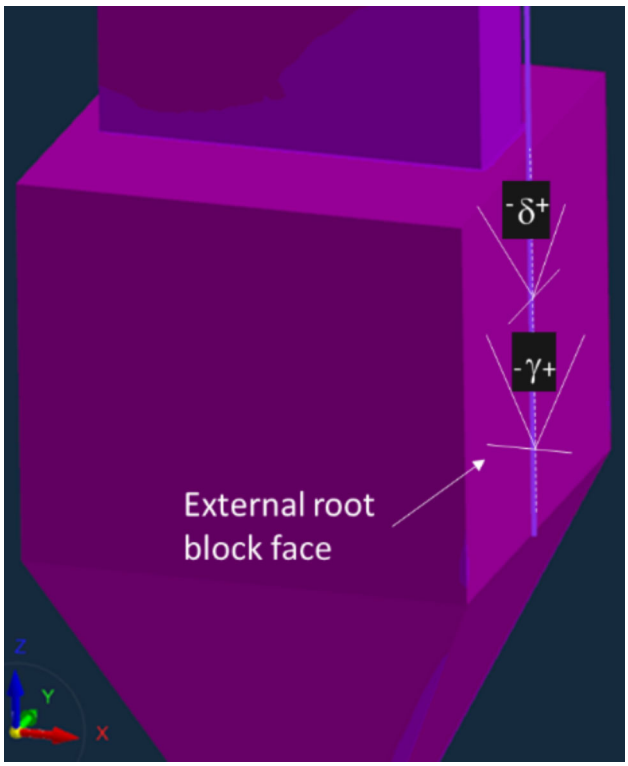


Fig. 2—Orientation measurement protocol for determination of crystal growth directions of inclination, $\gamma$, and rotation, $\delta$, relative to external root section face highlighted in Fig. 1.

with an open baffle freckle chains formed, ranging in number between three and eleven. Figure 3 shows representative examples revealed by etching. In several castings two or more chains were observed to merge, *e.g.* Figure 3(b); under these circumstances the maximum number of freckle chains formed prior to such events was recorded. As the number of freckle chains increased the height at which they formed above the delta decreased from 19- to 4 mm.

The orientations of each single-crystal casting relative to the external face on which freckles were observed are reported in Table II, along with the number of freckles. Measured inclinations of the upward growth direction to the external face ranged between + 23.3 deg (converging) to − 28.5 deg (diverging).

Figure 4 plots the number of freckle chains as a function of the inclination of the ⟨001⟩ upward growth direction ($\gamma$). It is immediately obvious that the number of freckles is strongly dependent on grain orientation, orientations in which the primary stems are convergent to the external face resulting in greater numbers of freckles. For any given orientation an upper limit is observed to the number of freckles formed. In the range $-10 \text{ deg} < \gamma < 10$ deg, the maximum number of freckles increases almost monotonically with angle from three to eleven, beyond which further convergent inclination results in no further increase in freckle count. The minimum spacing between adjacent chains was 3 mm.

Representative metallographic sections from larger areas prepared local to the region of freckle formation are shown in Figure 5. The PDAS measured using the Warnken–Reed method[16] yields mean and median spacings of 321 and 317 $\mu$ for the tight baffle and 585 and 562 microns, respectively, with the open baffle.

## IV. SOLIDIFICATION CONDITIONS LEADING TO FRECKLE FORMATION

In this section, we establish the solidification conditions local to the root block sections of the castings on which freckle chains occurred for both the open and tight baffles using ProCAST casting modelling software. Due to symmetry conditions it was only necessary to model one sixteenth of the mould. Casting conditions were as reported previously in Table I. Material properties and boundary conditions are proprietary to Rolls-Royce plc. Within the root block section key growth parameters of thermal gradient, $G$, and downward inclination of the liquidus isotherm to the external face, $\theta$, were obtained for the mid-plane radial section along with liquidus isotherm velocity.

Figures 6(a) and (b) show the fraction solid of a section through tight and open baffle castings on the mid-radial plane at a time when the liquidus isotherm is proximal to the location of freckle chain sources on the external face [white arrow in Figure 6(a)]. Figure 6(c) plots $G$ and $\theta$, the latter reported as positive when sloping downwards away from the external face, and Figure 6(d) shows the upward liquidus isotherm velocity, $v$.

It is clear that the open baffle both degrades the thermal gradient achieved with respect to the tight baffle from ca. 2- to 2.5 °C/mm to 1- to 1.2 °C/mm, whilst the corresponding liquidus slope increases by approximately 5 deg at all heights. As the liquidus isotherms advances upwards through the root section, $\theta$ decreases. At a height of 10 mm on the root block, the resulting cooling

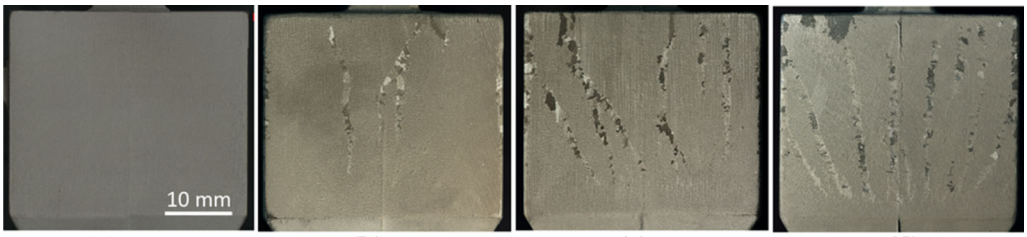


Fig. 3—Representative examples of castings with (*a*) tight baffle on no freckle chain defects and (*b*) through (*d*) open baffle with 3, 6, and 11 freckle chains, respectively.

**Table II. Measured Orientations and Freckle Counts on the External Root Block Face of Castings Produced Using Tight and Open Baffle Configurations**

| | | Grain Orientation (Deg) | | | | Grain Orientation (Deg) | |
|---|---|---|---|---|---|---|---|
| Baffle Condition | Freckle Count | $\gamma$ | $\delta$ | Baffle Condition | Freckle Count | $\gamma$ | $\delta$ |
| Tight | 0 | − 0.9 | − 1.5 | open | 4 | − 7.8 | 1.7 |
| Tight | 0 | − 0.3 | 0.8 | open | 10 | 13.3 | − 2.7 |
| Tight | 0 | − 13.7 | 7.7 | open | 5 | − 8.3 | − 3 |
| Tight | 0 | 1.3 | − 9.8 | open | 9 | 10.1 | 4.3 |
| Tight | 0 | 7.7 | 5.1 | open | 9 | 6 | 10.4 |
| Tight | 0 | − 3.7 | − 15.5 | open | 9 | 18.6 | 8.4 |
| Tight | 0 | − 19.6 | − 13.3 | open | 8 | 17.1 | − 1.7 |
| Tight | 0 | 2 | 0.6 | open | 3 | − 19 | − 9 |
| Tight | 0 | − 5.6 | 4.1 | open | 3 | − 18.5 | − 9 |
| Tight | 0 | − 7.8 | − 7.6 | open | 11 | 16.9 | 17 |
| Tight | 0 | − 10 | − 12.1 | open | 8 | 6.4 | 3.1 |
| Tight | 0 | 0.6 | 0.5 | open | 5 | 0.1 | 2.9 |
| Tight | 0 | 2.1 | − 16.6 | open | 11 | 18.1 | 10.7 |
| Tight | 0 | − 10.8 | − 12.3 | open | 11 | 10.1 | − 15.5 |
| Tight | 0 | 2.9 | 3.8 | open | 7 | 0.5 | 0.5 |
| Tight | 0 | − 7.6 | − 3.7 | open | 4 | − 3 | 5.1 |
| Tight | 0 | − 36.3 | − 6.3 | open | 7 | − 0.4 | 5.2 |
| Open | 4 | − 6.6 | 7.2 | open | 4 | − 3.5 | 12 |
| Open | 9 | 6.8 | 7.4 | open | 4 | − 4.2 | 0.7 |
| Open | 3 | − 7.6 | 6.4 | open | 6 | − 2.2 | 4.3 |
| Open | 10 | 9.3 | 9.1 | open | 8 | 1.8 | 9.9 |
| Open | 4 | − 0.4 | 1.7 | open | 8 | 3.8 | − 2.3 |
| Open | 5 | − 2.2 | 4.9 | open | 6 | − 4 | − 1.5 |
| Open | 6 | − 1.7 | − 3.2 | open | 4 | − 5.1 | − 1.5 |
| Open | 6 | 2.7 | − 0.8 | open | 6 | − 2.3 | 4.6 |
| Open | 10 | 17.2 | − 9.1 | open | 6 | 0.7 | 5.8 |
| Open | 3 | − 26.4 | − 24.3 | open | 4 | − 3.3 | − 5.9 |
| Open | 11 | 23.3 | 14.5 | open | 6 | − 1.3 | − 2.7 |
| Open | 6 | − 28.5 | − 22.3 | | | | |

rates of tight and open baffles are calculated to be 0.17- and 0.07 °Cs$^{-1}$, respectively, falling between the threshold of 0.1- to 0.14 °Cs$^{-1}$ that delineates freckling and non-freckling growth conditions,[4–6] supporting the absence of freckling in castings made with the tight baffle. Similarly, for the tight and open values $G^{-0.5}v^{-0.25}$ calculated at a height of 10 mm in the root block yields values of 0.71- and 1.22 cm$^{1/4}$ s$^{1/4}$ K$^{-1/2}$, respectively, these falling either side of the threshold of ~ 1 set out in.[17]

However, unsurprisingly, no evidence was found that may account for the differing severity of freckling in the open baffle castings, other than the experimentally observed effect of crystal orientation.

## V. ANISOTROPIC PERMEABILITY-BASED MODEL

In this section, we seek to rationalise the differing number of freckle chains formed in the open baffle castings by exploring the effect of anisotropic

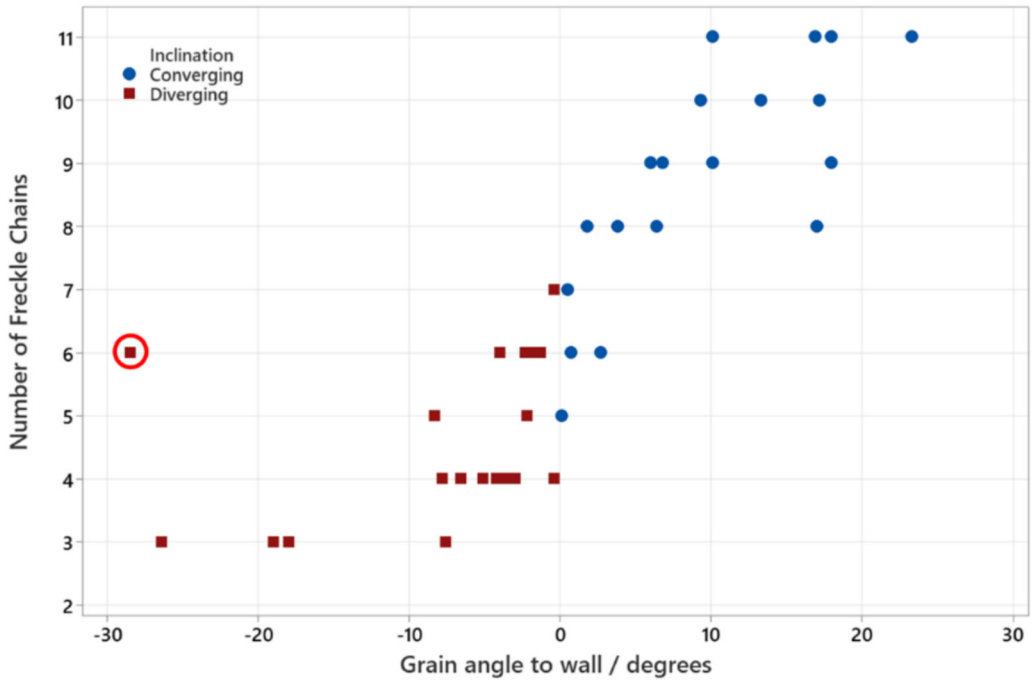


Fig. 4—Plot of dependency of the number of observed freckle chains as a function of ⟨001⟩⟨001⟩ crystal inclination ($\gamma$) relative to the external root block face of open baffle castings.

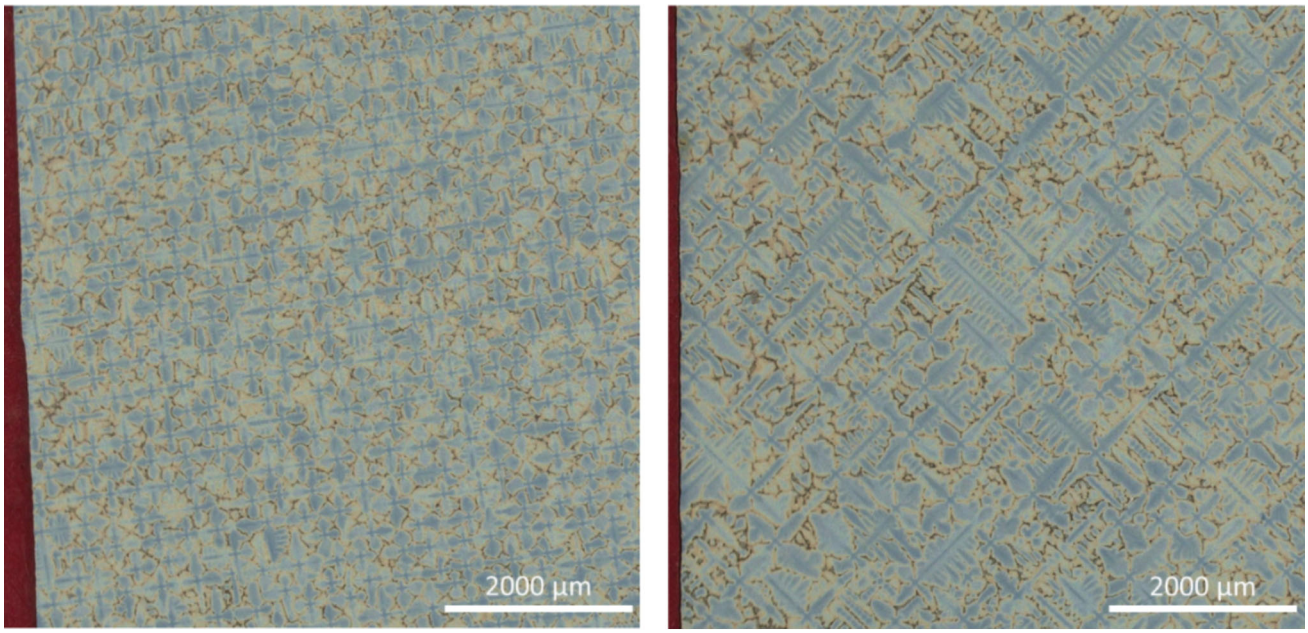


**(a)** **(b)**

Fig. 5—Transverse optical micrographs of structure in root block at a height of 7 mm above the delta. (*a*) Tight baffle and (*b*) open baffle. External root block face is to left of each image.

permeability in the semi-solid region to resist inward flow of liquid that sustains upward escaping streams of buoyant solute-enriched liquid local to dendrite tips. An expression is developed to calculate explicitly the total conductance to flow of any direct pathway of length $L$ from the liquidus iso-surface to the source of a solute plume at the wall in the mushy zone at some fraction solid $fs_{pl}$, from which a freckle may subsequently form. We also report results of freckle composition that are pertinent to application of the model before calculation of flow conductance through differing regions of the semi-solid.

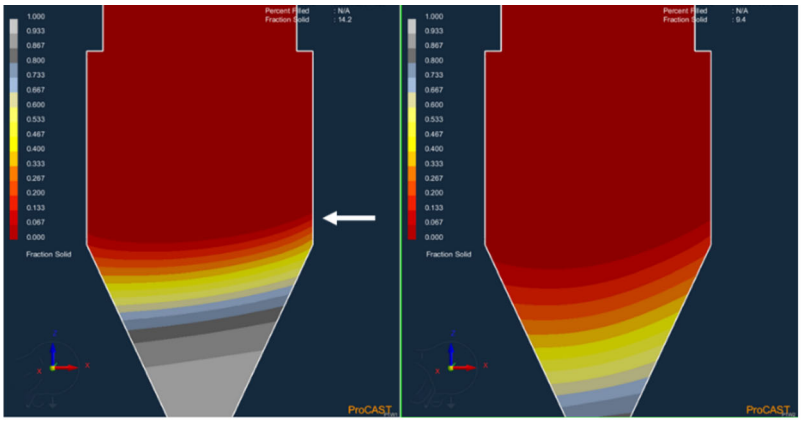


(a) (b)

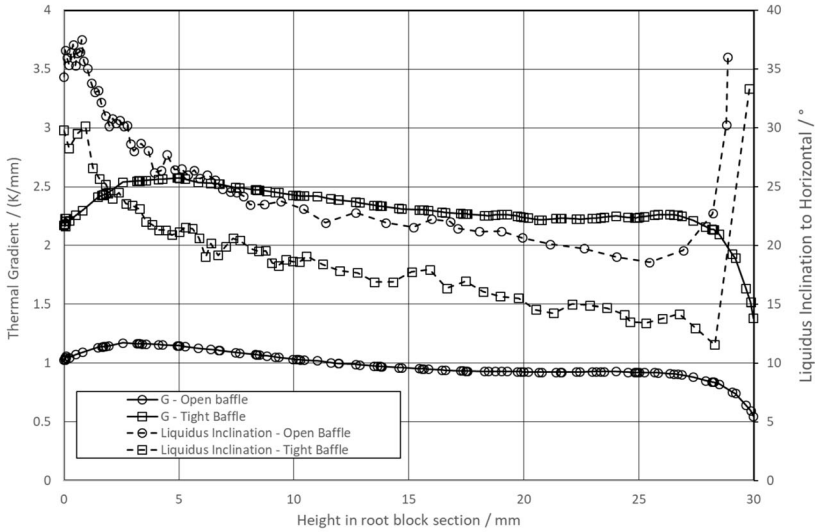


(c)

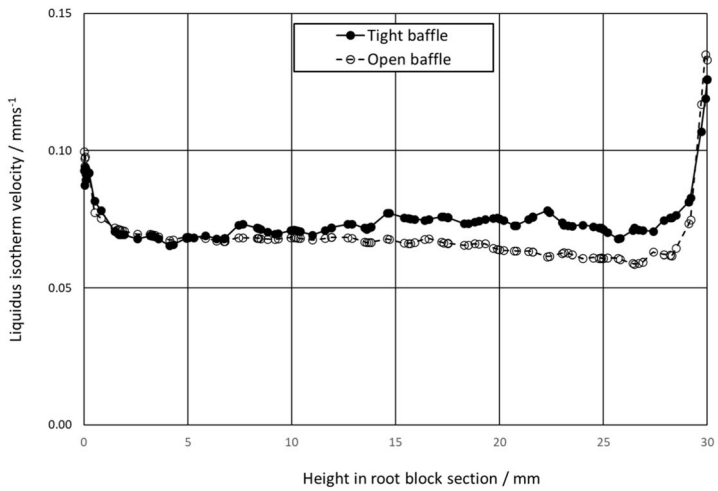


(d)

Fig. 6—(*a*) and (*b*) ProCAST model plots of fraction solid on the radial mid-plane sections of tight and open baffle castings showing delta, root block and lower airfoil when liquidus isotherm is proximal to location in which freckles form. Arrow in (a) indicates external casting face where freckles form. (*c*) Extracted thermal gradient and downward liquidus isotherm inclination at the external root block face as a function of height and (*d*) liquidus isotherm velocity.

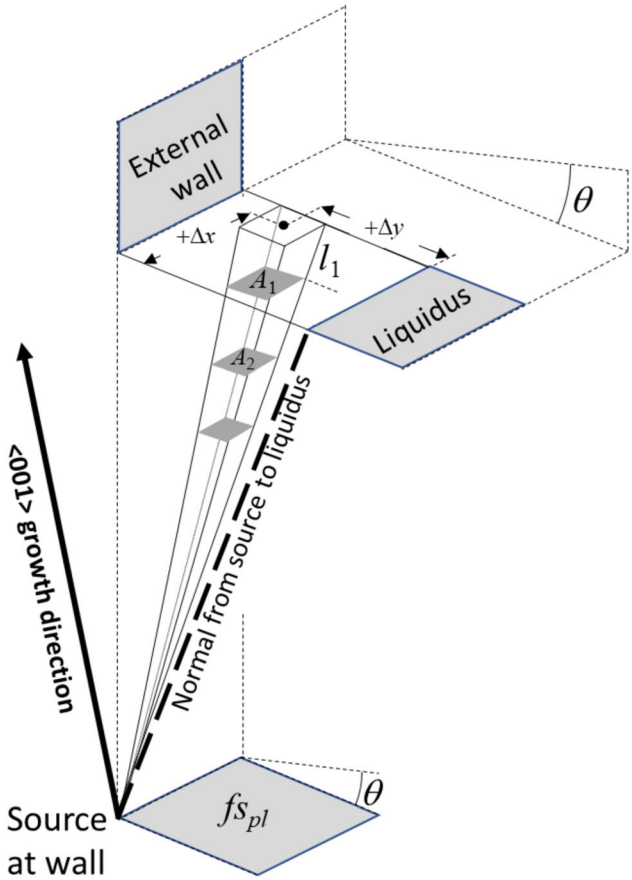


Fig. 7—Schematic diagram showing definition of frustum extending from the liquidus plane towards the source of an uprising thermosolutal plume responsible for freckle formation. The frustum is decomposed in to a series of frusta of progressively smaller cross-section $A_1$, $A_2$, …, $A_n$.

## A. *Model Formulation*

In the calculation domain, the liquidus surface is assumed to be of constant downward slope away from the mould wall with angle $\theta$. It is discretised to generate of a series of square based inclined frusta, converging on the freckle source. Each frustum terminates at a distance 0.1 $L$ from the mould wall—a requirement to avoid singularity in the calculation described below. The conductance of the channel formed by each frustum is calculated, and a criterion applied that determines if the flow path through that individual frustum is one within which flow will arise. For channels in which flow arises the conductances are summed piecemeal to obtain a total conductance. Figure 7 shows schematically a frustum within the semi-solid volume and a series of frusta formed by geometric decomposition.

To calculate the permeability, we select the anisotropic model for dendritic solidification reported in,[15] determining the parallel and transverse components of permeability, $\kappa_P$ and $\kappa_T$, to be calculated from the solidification conditions

$$\kappa_P = 0.0194\left[\frac{\lambda_2}{1+(\lambda_2/\lambda_1)}\right]^2\frac{(1-f_s)^3}{f_s^2} \quad [2]$$

$$\kappa_T = 0.0097\left[\frac{\lambda_2}{1+(\lambda_2/\lambda_1)+2(\lambda_2/\lambda_1)^2}\right]^2\frac{(1-f_s)^3}{f_s^2} \quad [3]$$

where $\lambda_1$ is the primary dendrite arm spacing, $\lambda_2$ is the secondary dendrite arm spacing, and $f_s$ is the fraction solid.

$\lambda_1$ is obtained from sectioning castings and for the purposes of calculation considered invariant with $f_s$, whilst the instantaneous $\lambda_2$ is calculated from the relationship derived experimentally in Ref. [18] wherein

$$\lambda_2 = 6.7t_{local}^{0.465} \quad [4]$$

and $t_{local}$ is the local time of growth of solid within the liquid. This is determined from

$$t_{local} = \frac{D}{v} \quad [5]$$

where $D$ is the distance of the calculation point below the liquidus isotherm in the z-direction.

Table III summarises calculated values of $\kappa_P$ and $\kappa_T$ and their ratios as a function of fraction solid. Similar proportionality of permeability has been reported in Ref. [19] for the Al–3Cu alloy.

To obtain the permeability of flow in the direction of the axis of each frustum, which is a function of crystal orientation $\gamma$ and $\delta$, a method equivalent to Lamé's stress ellipsoid construction was applied in the form of a prolate spheroid with $\kappa_P$ aligned to the measured $\langle 001\rangle$ primary dendrite growth direction.

The effective conductance, $C$, along each frustum formed from coordinate $\Delta_x$, $\Delta_y$ lying on the liquidus was calculated. For each segment 1 to $n$ of length $l$ and cross-section area $A$, the summed net conductance $C_{eff_{\Delta x,\Delta y}}$ is given by

$$C_{eff_{\Delta x,\Delta y}} = \frac{l_1 + l_2 + \ldots + l_n}{\frac{l_1}{\kappa_1 A_1} + \frac{l_2}{\kappa_2 A_2} + \ldots + \frac{l_n}{\kappa_n A_n}} \quad [6]$$

From consideration of the relative ratios of longitudinal versus transverse permeability (Eqs. [2] and [3]) which are always > 2 it is clear the summation of all pathways to the source of the freckle within the semi-solid would result in a maximum when the primary stem falls perpendicular to the liquidus isotherm, rather than convergent to the external wall. Instead, we invoke a criterion that only those flow paths satisfying either one of two criteria are those along which flow to the source of the freckle arises. This is postulated without prior evidence and is one of several that were considered and founded on the contention that only those flow channels whose conductance is greater than that of the shortest flow path length, defined by the normal to the liquidus from the freckle source, will result in flow. Thus, the criterion is as follows:

**Table III. Calculated Permeability Coefficients as a Function of Fraction Solid in the Directions Parallel ($\kappa_P$) and Transverse ($\kappa_T$) to the Primary Dendrite Stem and Anisotropy Ratio $\kappa_P/\kappa_T$**

| Experiment | Fraction solid | $\kappa_P/m^2$ | $\kappa_T/m^2$ | Anisotropy ratio $\kappa_P/\kappa_T$ |
|---|---|---|---|---|
| Tight Baffle (No Freckles) | 0.01 | 2.81E−08 | 1.40E−08 | 2.01 |
| | 0.02 | 1.26E−08 | 6.24E−09 | 2.02 |
| | 0.03 | 7.77E−09 | 3.82E−09 | 2.03 |
| | 0.05 | 4.09E−09 | 1.99E−09 | 2.05 |
| | 0.1 | 1.56E−09 | 7.43E−10 | 2.10 |
| | 0.2 | 4.83E−10 | 2.21E−10 | 2.18 |
| | 0.3 | 1.98E−10 | 8.75E−11 | 2.26 |
| | 0.4 | 4.32E−11 | 2.01E−11 | 2.15 |
| | 0.5 | 1.92E−11 | 8.76E−12 | 2.19 |
| Open Baffle (Freckles) | 0.01 | 2.69E−08 | 1.34E−08 | 2.01 |
| | 0.02 | 1.21E−08 | 5.98E−09 | 2.02 |
| | 0.03 | 7.44E−09 | 3.66E−09 | 2.03 |
| | 0.05 | 3.92E−09 | 1.91E−09 | 2.05 |
| | 0.1 | 1.50E−09 | 7.15E−10 | 2.10 |
| | 0.2 | 4.64E−10 | 2.13E−10 | 2.18 |
| | 0.3 | 1.91E−10 | 8.46E−11 | 2.25 |
| | 0.4 | 8.43E−11 | 3.63E−11 | 2.32 |
| | 0.5 | 3.70E−11 | 1.54E−11 | 2.39 |

Calculations were made using Eqs. [2] through [4] and casting process parameters in Table IV.

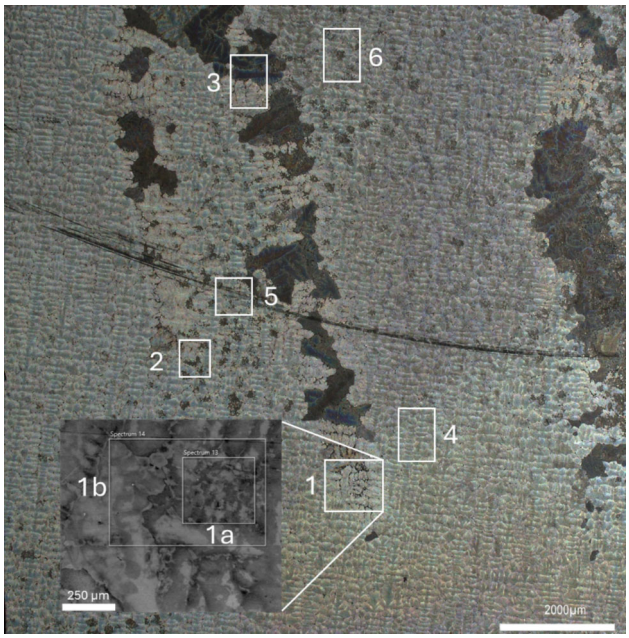


Fig. 8—Locations of EDS analysis of compositions in locations local to freckle chain initiation point (1), within the developed freckle chains (2,3) and single-crystal matrix (4,5,6).

1. Flow arises along the shortest path between the source of the solute plume within the semi-solid and the liquidus, *i.e.* the normal to the liquidus, with calculated conductance $C_N$.
2. Flow will also arise in any other frustum if it has permeability $C_{eff_{\Delta x,\Delta y}}$ greater or equal to $C_N$.

The total conductance for flow to the freckle, $C_{freck}$, is thus obtained by summing all active flow paths assuming flow would arise as series of independent paths within the semi-solid as a consequence of a common pressure differential.

Table IV reports the material properties and process parameters used for calculation of $C_{eff_{\Delta x,\Delta y}}$ and their sources.

## B. *Freckle Characterisation*

In Ref. [17], it was concluded based on Rayleigh number that the critical fraction solid at which solute plumes are formed lies in the region 0.1 to 0.2. More recently, direct radiographic observation of thermally constrained solidification of an 0.3 mm thickness sheet of CMSX-4 suggested flow to the wall may occur at temperatures of 40 °C below the liquidus[3] with subsequent solidification within the channels resulting in equiaxed grains. Similarly, modelling has predicted an upward flow along the length of channels at the cooled wall and dendrite remelting.[20] Further, modelling of nickel superalloy castings in which freckles form has also predicted flow that could sustain a solute plume persists for approximately half of the solidification interval between liquidus and the onset of the eutectic transformation.[21]

To investigate the composition of the liquid from which the freckle grains formed in this study measurements were made at the external surface by EDS. Areas within the point of initiation, freckle channel and matrix were studied, Figure 8. Results are reported in Table V.

Using JMatPro® release 10.2, Gulliver–Scheil calculations were performed to establish the fraction solid in the alloy matrix (Sample 4, Table V) at which the computed liquidus temperature of the freckle chains (1b, 2, 3 in Table V) arises. Calculation predicts $f_s$ in the range of 0.51 to 0.55 for the respective analyses and 0.53 for the averaged compositions.

Table IV. Material Properties, Process, and Calculation Parameters Used to Determine $\kappa_{freck}$ for Each Casting

| Model Data | | | Source |
|---|---|---|---|
| Material, CMSX-4 | Rate of evolution of solid, $d_{fs}/dT df_s/dT$ | 0.0251 $K^{-1}$ | JMatPro modelling, interval 0 to 0.25 fs |
| | Fraction solid at source of plume, $fs_{pl}$ | 0.15, 0.45 | Ref. [17] maximum calculated *Ra* and nominal location within bulk |
| | Primary dendrite arm spacing, *PDAS* | 317 $\mu$m | Tight baffle, experimental measurement, this paper |
| | Primary dendrite arm spacing, *pdas* | 562 $\mu$m | Open baffle, experimental measurement, this paper |
| | Grain angle and rotation to external root block face | From Table II | Laue measurements |
| | Half freckle separation, *d* | $2 \times 10^{-3}$ m | Typical from experimental observations in this study |
| Casting Process | Withdrawal velocity, *v* | $6.3 \times 10^{-5}$ $ms^{-1}$ | Process setup |
| | Liquidus slope, $\theta$, tight baffle | 18 deg | ProCAST model, 10 mm height in root block |
| | liquidus slope, $\theta$, open baffle | 25 deg | ProCAST model, 10 mm height in root block |
| | Thermal gradient,$dT/dZ$ | 2450 $Km^{-1}$ | ProCAST model, tight baffle, 10 mm height in root block |
| | Thermal gradient,$dT/dZ$ | 1050 $Km^{-1}$ | ProCAST model, open baffle, 10 mm height in root block |
| Calculation | Number of frustra used for calculation | 5 | $f_s$ intervals 0–0.1, 0.1–0.3, 0.3–0.5, 0.5–0.7, 0.7–0.9 |
| | Number of cells to discretise liquidus surface | $20 \times 10$ | width $\times$ length |

Therefore, two scenarios are assessed, one locating the source at the wall at fraction solid 0.15 to reflect the condition where the initial flow channel may start to form, and the second at fraction solid 0.45 to reflect flow within the greater volume that is required to sustain a channel that forms freckles.

### C. *Calculated Flow Conductance*

Figures 9(a) and (b) plot the calculated conductance for freckle channel formation, $C_{freck}$, as a function of crystal orientation for both tight and open baffles at fractions solid 0.15 and 0.45, respectively. It is seen that, despite overlapping distributions of orientations, there is clear separation between $C_{freck}$ of tight and open baffles at both fractions solid used in calculation. For $fs_{pl}$ 0.15, the maximum calculated conductance of the tight baffle castings, in which no freckles arose, is $0.365 \times 10^{-14}$ $m^3s^{-1}$, whereas the minimum permeability of the castings made with open baffle is $0.458 \times 10^{-14}$ $m^3s^{-1}$ and in which freckles formed. Therefore, if all other factors affecting the likelihood of freckling are second order in nature for this particular alloy, the critical conductance $C_{freck(crit)}$ lies between these two values and may be deduced with relatively low uncertainty. A similarly discriminating result is obtained for calculations made using $fs_{pl}$ 0.45, albeit the calculated conductances are reduced fivefold. Figures 9(c) and (d) plot the number of freckles as a function of $C_{freck}$ for all castings.

It is observed that there exists an upper limit to the number of freckles formed (11), further increases in $C_{freck}$ having no effect. For $fs_{pl}$ 0.15 the system saturates when $C_{freck}$ exceeds $3.2 \times 10^{-14}$ $m^3s^{-1}$ and $0.69 \times 10^{-14}$ $m^3s^{-1}$ for $fs_{pl}$ 0.45. The minimum separation of approximately 3 mm indicates how localised solute flow is, restricted to two or three primary dendrites to either side. Similar observations of very localised solute plumes were reported in Reference 3. However, above these threshold values fewer than 11 freckles may be formed. This aligns with the widely advanced contention that freckling remains to some degree a stochastic response to material and process parameters influenced, perhaps, by localised variation in microstructural parameters *PDAS* and *SDAS*. One such source of local variation of response may be the range of possible primary dendrite stable growth spacings.[22] This is explored further below using Monte Carlo modelling.

Despite considerations of potential sources of variability in the number of freckles arising, the contention that $C_{freck}$ calculated via the method set out allows prediction of the likelihood of freckling is supported further by consideration of the apparent outlying result in Figure 4, ringed in red, where six freckles were observed with a grain inclination of − 28 deg away from the external face. When freckle count is plotted as a function of $C_{freck}$ the data lies far more closely within the general population of results, Figure 9(c) and (d).

Table V. EDS Measurements of Compositions at Locations Shown in Fig. 8

| Sample | Al | Ti | Cr | Co | Ni | Mo | Ta | W | Re | Location |
|---|---|---|---|---|---|---|---|---|---|---|
| 1a | 6.18 | 1.44 | 7.81 | 9.53 | 60.44 | 1.15 | 9.08 | 4.37 | 0.00 | Freckle source |
| 1b | 6.09 | 1.21 | 7.50 | 9.65 | 58.48 | 0.92 | 8.81 | 5.65 | 1.68 | Freckle source |
| 2 | 6.42 | 1.21 | 7.46 | 9.80 | 60.88 | 0.95 | 8.28 | 5.00 | 0.00 | Freckle |
| 3 | 6.20 | 1.08 | 7.29 | 9.90 | 60.57 | 0.78 | 8.76 | 5.43 | 0.00 | Freckle |
| 4 | 5.03 | 0.77 | 7.08 | 9.82 | 57.94 | 0.72 | 7.07 | 8.26 | 3.30 | Matrix |
| 5 | 5.72 | 0.81 | 7.24 | 9.92 | 58.56 | 0.74 | 6.63 | 7.39 | 2.99 | Matrix |
| 6 | 5.40 | 0.93 | 7.12 | 9.95 | 58.97 | 0.79 | 6.60 | 7.20 | 3.03 | Matrix |

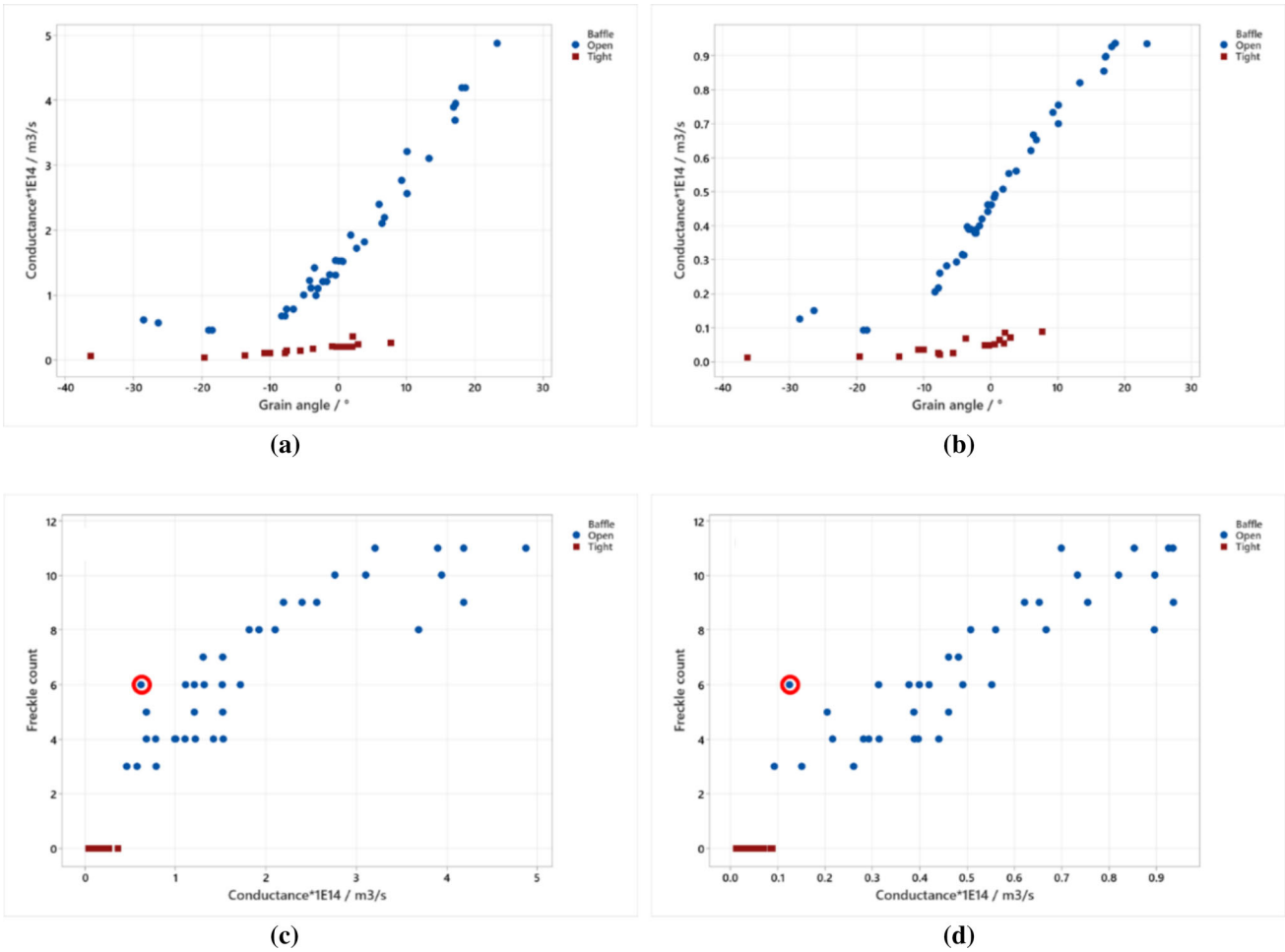


Fig. 9—Calculated freckle flow path conductance, $C_{freck}$, of open and tight baffle castings as a function of $\gamma$ (x-axis) and $\delta$ (not plotted) for $fs_{pl}$ 0.15 (*a*) and 0.45 (*b*) where a positive grain angle indicates primary stem growth convergent to the wall, and freckle counts as a function of $C_{freck}$ for $fs_{pl}$ 0.15 (*c*) and 0.45 (*d*). Red circles in (b) and (d) refer to result circled in Fig. 4.

### D. *Applicability of Conductance Model to Plume and Freckle Prediction in Single-Crystal Castings*

Despite the apparent congruence between results obtained using fraction solid 0.15 and 0.45 in identification of a threshold value of $C_{freck}$ above which freckles arise, the absolute magnitude $C_{freck}$ is reduced nearly fivefold as at higher $f_s$, despite the increased area of the liquidus through which flow may arise. Instead, it is proposed that flow channel formation and freckle defect formation proceeds via a two-stage process, Figure 10.

Firstly [Figure 10(a)], liquidus slope, crystal orientation and growth conditions at time $t_3$ are favourable to initiation of thermosolutal flow local to the dendrite tip(s) at the wall leading to formation of a groove (b) between the mould wall and adjacent growing primary stem. With upward solidification and sustained flow the groove transitions into a channel (c). This is fed through

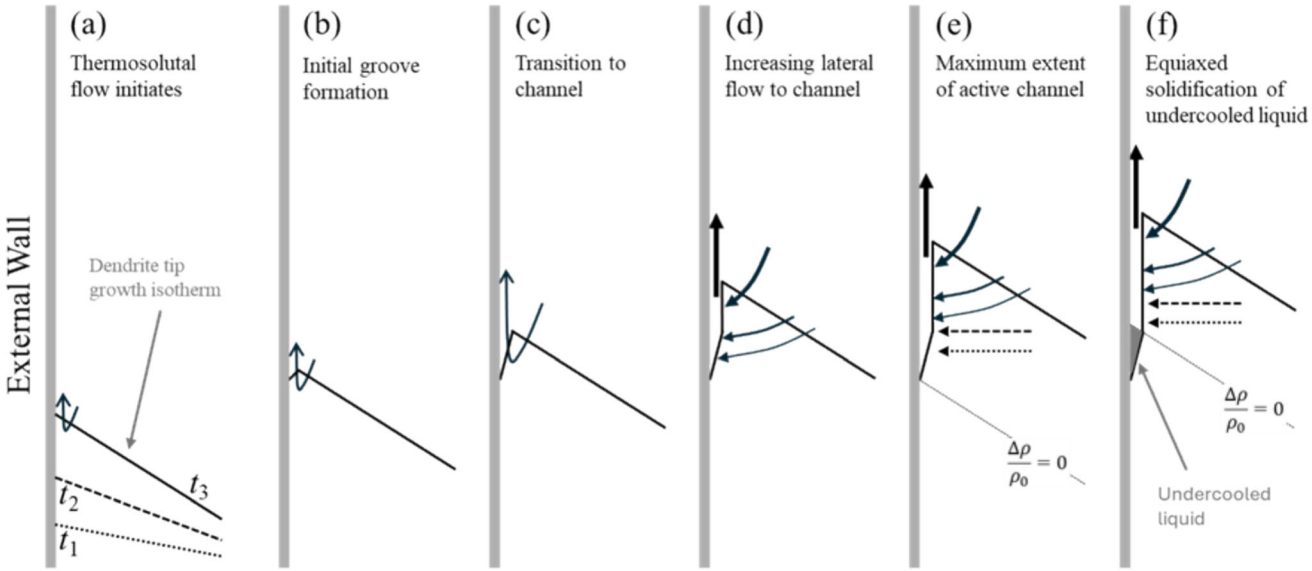


Fig. 10—Proposed sequential development of a thermosolutal flow channel and transition in to a freckle chain wherein (*a*) liquidus slope, crystal orientation and growth conditions at time $t_3$ are favourable to initiation of thermosolutal flow local to the of dendrite tips, (*b*) groove formation, (*c*) the groove transitions into a channel with more extensive lateral liquid movement (*d*). When the partitioned liquid density exceeds that of the bulk above flow ceases (*e*) after which the liquid becomes undercooled with risk of secondary equiaxed grains (*f*).

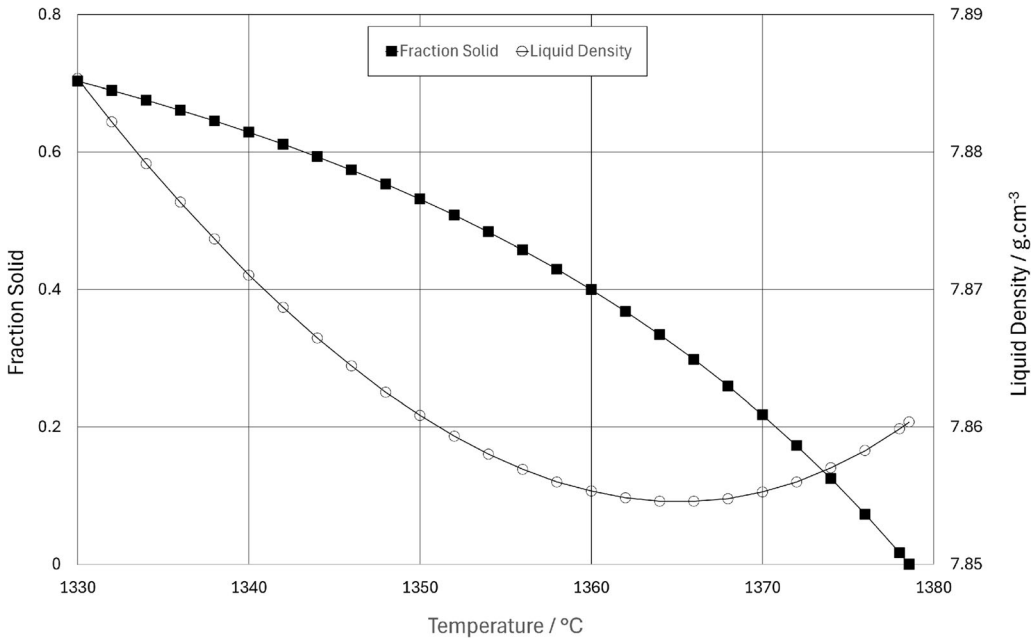


Fig. 11—Calculated fraction solid and liquid density of alloy of composition reported for Area 4 in Table V.

more extensive lateral liquid flow (d). When the partitioned liquid composition flowing to the base of the channel is of density greater than that of the overlying bulk liquid upward flow from this region ceases (e). Subsequent upward motion of the thermal field causes the liquid to become undercooled with risk of nucleation of secondary grains or recalescence induced remelting of side arms during solidification.

To test this hypothesis Figure 11 plots the fraction solid and liquid density obtained using the JMatPro® calculation reported above. The density difference becomes positive at fraction solid 0.53, corresponding closely with the measured freckle composition (Table V(1b)).

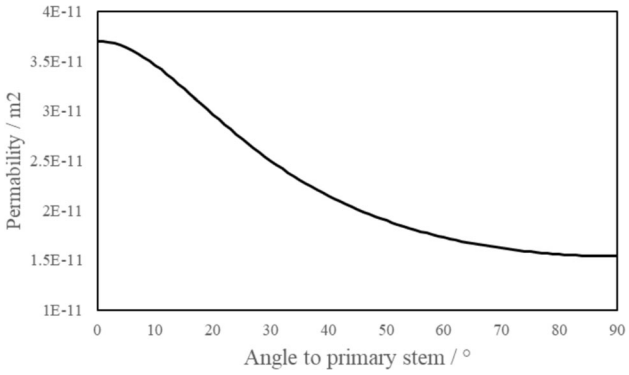


Fig. 12—Permeability as a function of inclination of flow direction to the primary dendrite stem at fraction solid, $f_s$, 0.5.

**Table VI. Variables Integrated in to Monte Carlo Model of $C_{freck}$**

| Parameter | Range |
|---|---|
| Liquidus Slope, $\theta$/rad | 0.0001–0.7 |
| Grain Angle to Wall, GAMMA/Rad | − 0.4 to 0.4 |
| Grain Rotation to Wall, DELTA/Rad | − 0.4 to 0.4 |
| Temperature Gradient, $G$/Km$^{-1}$ | 700–1500 |
| PDAS/$\mu$m | 250–700 |
| Liquidus Isotherm Velocity, v/$\mu$ms$^{-1}$ | 50–150 |
| Fraction Solid at Plume Source, $fs_{pl}$ | 0.15–0.45 |

## E. *Consideration of the Role of Crystal Orientation on Flow at High Fraction Solid*

It has been demonstrated that flow conductance local to the tips of the dendrites where initial solute plumes form is highly sensitive to crystal orientation relative to the external wall. Using values of permeability reported for the open baffle condition in Table III at $f_s$ 0.5 the effect of orientation dependence of permeability was calculated using Lamé's ellipsoid and plotted in Figure 12. It is clear that transverse permeability in the range of angles 70 to 90 deg, corresponding to primary stem inclinations of 20 to 0 deg that encompasses almost all castings produced is effectively invariant. This suggests that the dominant mechanism determining the number of freckles formed due to thermosolutal channel formation is the flow local to the dendrite tips, i.e. Figure 10 (a) to (c), as predicted by Rayleigh number, but is highly sensitive to grain inclination.

The implications for casting process design profound—there will exist preferred grain orientations within a component that are less prone to freckling. However, the sensitivity of the result to minor variation of orientation is surprising.

In the next section we extend the model to investigate the sensitivity of $C_{freck}$ to variations in microstructural and process parameters.

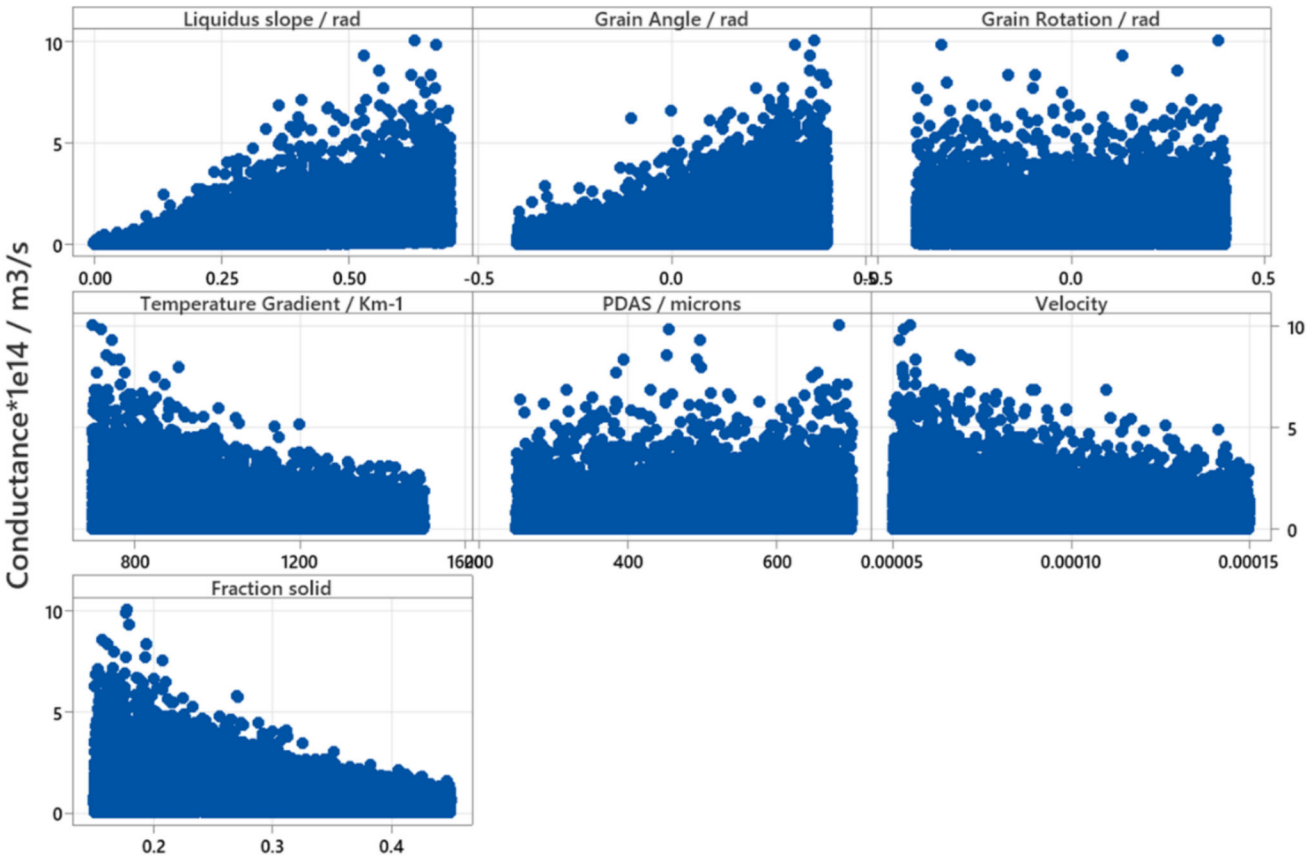


Fig. 13—Single factor plots of conductance, $C_{freck}$, calculated using variables set out in Table VI.

## VI. MONTE CARLO MODEL OF $C_{FRECK}$ SENSITIVITY TO MATERIAL AND PROCESS PARAMETERS

The explicit calculation of flow conductance at the wall of single-crystal castings was extended to a Monte Carlo modelling framework within which the parameters set out in Table VI were varied in random combination. The half plume spacing was fixed at 2 mm. 20,000 combinations were used. Single factor plots of $C_{freck}$ are shown in Figure 13.

On inspection of Figure 13, with the exception of grain rotation and PDAS, it is clear that either an upward or downward sloping upper bound to the plotted values indicates that $C_{freck}$ is affected by the variable. Within the range of each value applied, and based on the gradient of the upper bound the sensitivities of $C_{freck}$ can be grouped as follows: (i) most significant—grain angle, thermal gradient, liquidus slope, and fraction solid at which the freckle initiates; (ii) moderately significant—withdrawal velocity; and, surprisingly; and (iii) least significant—PDAS alongside grain rotation.

The opportunity presented by the model is clear, insomuch that straightforward regression of response to the parameters studied can yield a tool for quantitative prediction of the likelihood of freckling. The outputs of this may then be applied to model based optimisation of casting processes to eliminate freckle defects when casting nickel base superalloy single crystals.

## VII. SUMMARY AND CONCLUSIONS

1. It has been shown that for a fixed set of casting conditions, the number of freckle chains formed during casting of nickel base superalloy single-crystal alloy CMSX-4 is strongly dependent on grain orientation. Convergence of the ⟨001⟩ upward growth direction with an external wall from which the liquidus isotherm slopes downward increases the likelihood and severity of freckle formation.
2. A model has been developed that rationalises the above, requiring explicit calculation of the effective conductance to flow through the semi-solid. This accounts for the anisotropic permeability of flow parallel and perpendicular to the primary dendrite growth direction, orientation of the grain within the casting, growth conditions and microstructure. By applying a newly defined criterion for flow within the semi-solid the model achieves good correlation with experimental results such that increasing conductance is predicted to result in increased numbers of freckle chains.
3. Flow through the semi-solid mush to the source of a solute plume terminates when the interdendritic liquid density exceeds that of the overlying bulk liquid.
4. Through application of a Monte Carlo model the effect of process and microstructural parameters has been investigated. Outputs of the study predict that the dominant factors controlling the likelihood of freckling are grain orientation relative the external face(s) of a casting, liquidus slope and thermal gradient. Primary dendrite arm spacing is predicted to only weakly affect the likelihood of freckling.


## ACKNOWLEDGEMENTS

This work was supported by Rolls-Royce plc; the Engineering and Physical Sciences Research Council [Grant Number EP/X025454/1, Advanced Research into Crystallographic Anisotropy & Nucleation Effects in single crystals (ARCANE)] and the Royal Academy of Engineering [Research Chair in Nickel-Based Superalloys for Next-Generation Aircraft Propulsion].


## DATA AVAILABILITY

The data supporting the findings of this study are available from the corresponding author upon reasonable request.

## CONFLICT OF INTEREST

On behalf of all authors, the corresponding author states that there is no conflict of interest.



## REFERENCES


1. J. Hong, D. Ma, J. Wang, F. Wang, B. Sun, A. Dong, F. Li, and A. Bührig-Polaczek: *Materials*. 2016. https://doi.org/10.3390/ma9110929.

2. N. Shevchenko, S. Eckert, S. Boden, and G. Gerbeth: *IOP Conf Ser Mater Sci Eng*, 2012. https://doi.org/10.1088/1757-899X/33/1/012035.
3. G. Reinhart, D. Grange, L. Abou-Khalil, N. Mangelinck-Noël, N.T. Niane, V. Maguin, G. Guillemot, C.A. Gandin, and H. Nguyen-Thi: *Acta Mater.*, 2020, vol. 194, pp. 68–79. https://doi.org/10.1016/j.actamat.2020.04.003.
4. S.M. Copley, A.F. Giamei, S.M. Johnson, and M.F. Hornbecker: *Transactions*, 1970, vol. 1, pp. 2193–2204.
5. T.M. Pollock, W.H. Murphy, E.H. Goldman, D.L. Uram, and J.S. Tu, in: Superalloy 1992, 1992.
6. R. Schadt, I. Wagner, J. Preuhs, and P.R. Sahm: in: Superalloy 2000, 2000.
7. R. Mehrabian, M.A. Keane, and M.C. Flemings: *Transactions*, 1970, vol. 1, pp. 3238–41.
8. P. Auburtin, S.L. Cockcroft, A. Mitchell: in: Superalloy 1996, 1996.
9. P. Auburtin, T. Wang, S.L. Cockcroft, and A. Mitchell: *Metall. Mater. Trans. B.*, 2000, vol. 31B, pp. 801–11.
10. R.A. Hobbs, S. Tin, and C.M.F. Rae: *Metall. Mater. Trans. A.*, 2005, vol. 36A, pp. 2761–73.
11. T.M. Pollock and W.H. Murphy: *Metall. Mater. Trans. A*, 1996, vol. 27A, pp. 1081–94.
12. J. Kozeny: *Wien*, 1927, vol. 136(2a), pp. 271–306.
13. D. Ma, M. Mathes, B. Zhou, and A. Bührig-Polaczek: *Adv. Mater. Res*, 2011. https://doi.org/10.4028/www.scientific.net/AMR.278.114.
14. A. Kao, N. Shevchenko, M. Alexandrakis, I. Krastins, S. Eckert, and K. Pericleous: *Philos. Trans. R. Soc. A*, 2019. https://doi.org/10.1098/rsta.2018.0206.
15. Y. Natsume, D. Takahashi, K. Kawashima, E. Tanigawa, and K. Ohsasa: *ISIJ Int.*, 2013, vol. 53, pp. 838–47. https://doi.org/10.2355/isijinternational.53.838.
16. N. Warnken and R.C. Reed: *Metall. Mater. Trans. A*, 2011. https://doi.org/10.1007/s11661-010-0544-4.
17. C. Beckermann, J.P. Gu, and W.J. Boettinger: *Metall. Mater. Trans. A*, 2000, vol. 31A, pp. 2545–57.
18. G. Matache, D.M. Stefanescu, C. Puscasu, and E. Alexandrescu: *Int. J. Cast Met. Res.*, 2016, vol. 29, pp. 303–16. https://doi.org/10.1080/13640461.2016.1166726.
19. Y. Mitsuyamaa, T. Takakib, S. Sakanea, Y. Shibutac, and M. Ohno: *Acta Mater.*, 2020, vol. 188, pp. 282–87. https://doi.org/10.1016/j.actamat.2020.02.016.
20. N. Rena, C. Panwisawas, J. Li, M. Xiaa, H. Dong, and J. Li: *Acta Mater.*, 2021, vol. 215, p. 117043. https://doi.org/10.1016/j.actamat.2021.117043.
21. H. Zhang, Y. Zhao, W. Xiong, D. Ma, A. Ludwig, A. Kharicha, and M. Wu: *Commun. Mater.*, 2024, vol. 5, p. 232. https://doi.org/10.1038/s43246-024-00672-4.
22. J.A. Warren and J.S. Langer: *Phys. Rev. E*, 1993, vol. 47, pp. 2702–13.